Supplemental Materials for "Climate & Ecology in the Rocky Mountain Interior After the Early Eocene Climatic Optimum"

Rebekah A. Stein[1,2], Nathan D. Sheldon[1], Sarah E. Allen[3], Michael E. Smith[4], Rebecca M. Dzombak[1], Brian R. Jicha[5]

Supplemental Tables:

Table S1: Paleosol features. Paleosols are stored in ESS labs at the University of Michigan, Ann Arbor, U.S.A.

Sample ID	Paleosol #	Depth (cm)	Horizon	Root traces, rhizoliths	Redox Haloes	Burrows	Peds	Color (descriptive + Munsell)	Texture
19BRWY1UA	1	0	A	Yes				5Y 6/1	
19BRWY1LA	1	-12	A	Yes			Yes	2.5Y 6/1	silt sandstone
19BRWY1LC	1	-18	C					dark brown, 10YR 5/2	silt sandstone, no bedding, not laminated
19BRWY2UA	2	0 to -5	A	Yes	Yes			green grey, 2.5Y 7/3	
19BRWY2UB	2	-25	B			Yes, up to 1cm		5Y 7/2	
19BRWY2MB	2	-50	B			Yes, up to 1cm		olive, 5Y 7/2	mudstone
19BRWY2LB	2	-75	B					2.5YR 7/3	
19BRWY2C	2	-85	C	Yes, very fine				dark grey, GLEY1 7/10Y	clay-silt to silty clay, laminated
19BRWY3UA	3	0	A	Yes				brown green, 5Y 7/2	
19BRWY3UB	3	-35	B					grey-brown, 5Y 8/1	silty mudstone
19BRWY3MB	3	-45	B					10YR 7/1	
19BRWY3C	3	-75	C					dark grey, 5Y 7/1	mudstone
19BRWY4UB1	4	0	B	Yes	Yes			10YR 7/2	sandy
19BRWY4UB2	4	-15	B					GLEY1 7/10Y	sandy mudstone
19BRWY4LB	4	-30	B					2.5Y 6/2	shale, mudstone
19BRWY4C	4	-60	C					5Y 8/1	shale, mudstone
19BRWY5UA	5	0	A	Yes				dark grey, green	silty mudstone
19BRWY5UB	5	-20	B	Yes				5Y 7/1	siltstone
19BRWY5MB	5	-35	B					5Y 7/2	
19BRWY5C	5	-80	C					dark grey, 5Y 6/1	massive fine sand mudstone
19BRWY6UA	6	0	A					10YR 7/1	
19BRWY6UB	6	-42	B					5Y 7/1	
19BRWY6MB	6	-72	B					5Y 7/2	shale, mudstone
19BRWY6C	6	-112	C					2.5Y 5/1	shale, mudstone

Table 2. Complete $^{40}Ar/^{39}Ar$ results

MAP 215-50

Laser - Single crystal fusion

Sample: BR-6 J-value: 0.0105317 ± 0.0000058 (2σ)

Material: sanidine and orthoclase

File	$^{40}Ar/^{39}Ar$	±1σ	$^{39}Ar/^{39}Ar$	±1σ	$^{36}Ar/^{39}Ar$	±1σ	$^{40}Ar^*/^{39}Ar_K$	± 2σ	% $^{40}Ar^*$	Age (Ma) ± 2σ (Ma)	K/Ca	$^{40}Ar^*$ (x e-15 mol)	Included in wtd. Mean
MAA3467	103.2380	± 0.2319	0.00155	± 0.00025	0.00026054	± 0.0000649	103.15989	± 0.46509	99.92	1346.26 ± 4.30	277.9	32.62	
MAA3468	6.2767	± 0.0127	0.00150	± 0.00033	0.00043156	± 0.0000597	6.14745	± 0.04359	97.94	114.83 ± 0.79	286.8	1.52	
MAA3470	122.0564	± 1.9798	2.98467	± 0.06722	0.00304601	± 0.0022998	121.63489	± 4.18671	99.45	1509.47 ± 35.38	0.1	0.72	
MAA3471	92.9050	± 0.2016	0.00261	± 0.00044	0.00051381	± 0.0000797	92.75144	± 0.40525	99.83	1247.47 ± 3.95	164.4	21.16	
MAA3473	2.6685	± 0.0087	0.01655	± 0.00077	0.00024881	± 0.0000818	2.59504	± 0.05174	97.25	49.36 ± 0.97	26.0	0.43	x
MAA3474	4.2453	± 0.0097	0.00143	± 0.00046	0.00017891	± 0.0000810	4.19148	± 0.05206	98.73	79.07 ± 0.96	300.9	0.78	
MAA3476	56.8838	± 0.1520	0.00408	± 0.00048	0.00027627	± 0.0000910	56.80121	± 0.30843	99.85	858.29 ± 3.72	105.3	9.56	
MAA3477	2.2931	± 0.0063	0.01234	± 0.00073	0.00006373	± 0.0000703	2.27457	± 0.04380	99.19	43.33 ± 0.82	34.9	0.46	
MAA3479	31.7415	± 0.0891	0.00453	± 0.00062	0.00050642	± 0.0001266	31.59023	± 0.19278	99.52	525.73 ± 2.79	95.0	3.52	
MAA3480	2.5574	± 0.0095	0.01244	± 0.00104	0.00000765	± 0.0001293	2.55560	± 0.07953	99.93	48.62 ± 1.49	34.6	0.29	x
MAA3482	2.5268	± 0.0065	0.00458	± 0.00046	0.00007726	± 0.0000657	2.50352	± 0.04131	99.08	47.64 ± 0.78	93.9	0.52	x
MAA3483	2.5697	± 0.0092	0.01166	± 0.00071	0.00007149	± 0.0001016	2.54879	± 0.06338	99.18	48.49 ± 1.19	36.9	0.34	x
MAA3485	2.5571	± 0.0078	0.01141	± 0.00086	0.00001604	± 0.0001028	2.55268	± 0.06332	99.83	48.56 ± 1.19	37.7	0.35	x
MAA3486	2.6850	± 0.0073	0.01448	± 0.00067	0.00020773	± 0.0000750	2.62366	± 0.04707	97.71	49.89 ± 0.88	29.7	0.48	
MAA3488	93.1071	± 0.2544	0.00297	± 0.00063	0.00021251	± 0.0001121	93.04351	± 0.51280	99.93	1250.32 ± 4.99	144.9	12.06	
MAA3489	2.6328	± 0.0091	0.01504	± 0.00079	0.00019441	± 0.0001136	2.57541	± 0.07018	97.82	48.99 ± 1.32	28.6	0.31	x
MAA3491	2.6102	± 0.0084	0.01021	± 0.00072	0.00020218	± 0.0000921	2.55008	± 0.05739	97.70	48.51 ± 1.08	42.1	0.39	x
MAA3492	11.2200	± 0.0382	0.00303	± 0.00087	0.00027801	± 0.0001359	11.13669	± 0.11103	99.26	203.01 ± 1.92	142.0	1.14	
									Weighted mean age (6 of 18):		48.48 ± 0.60	MSWD:	1.40

Laser - Single crystal fusion

Sample: BR-5 J-value: 0.0105317 ± 0.0000058 (2σ)

Material: sanidine and orthoclase

File	$^{40}Ar/^{39}Ar$	±1σ	$^{39}Ar/^{39}Ar$	±1σ	$^{36}Ar/^{39}Ar$	±1σ	$^{40}Ar^*/^{39}Ar_K$	± 2σ	% $^{40}Ar^*$	Age (Ma) ± 2σ (Ma)	K/Ca	$^{40}Ar^*$ (x e-15 mol)	Included in wtd. Mean
MAA3376	96.1168	± 0.2027	0.00307	± 0.00037	0.00055795	± 0.0000631	95.95010	± 0.40645	99.83	1278.40 ± 3.90	139.9	30.70	
MAA3377	4.6954	± 0.0071	0.00062	± 0.00015	0.00017428	± 0.0000333	4.64287	± 0.02431	98.88	87.39 ± 0.45	693.9	2.52	
MAA3379	64.0019	± 0.1045	0.00919	± 0.00050	0.00013895	± 0.0000563	63.96099	± 0.21162	99.94	942.68 ± 2.44	46.8	21.79	
MAA3380	12.5249	± 0.0250	0.01160	± 0.00070	0.00005171	± 0.0000966	12.50999	± 0.07627	99.88	226.55 ± 1.30	37.1	2.61	
MAA3382	4.6101	± 0.0088	0.00962	± 0.00037	0.00004221	± 0.0000484	4.59779	± 0.03382	99.73	86.56 ± 0.62	44.7	1.64	
MAA3383	22.8047	± 0.0417	0.00568	± 0.00034	0.00015340	± 0.0000525	22.75891	± 0.08895	99.80	393.30 ± 1.38	75.7	7.92	
MAA3385	85.0975	± 0.1457	0.00019	± 0.00019	0.00016558	± 0.0000464	85.04751	± 0.29253	99.94	1170.76 ± 2.97	2277.4	40.82	
MAA3386	9.6783	± 0.0181	0.00652	± 0.00028	0.00012046	± 0.0000538	9.64234	± 0.04831	99.63	177.04 ± 0.85	65.9	3.09	
MAA3388	12.8873	± 0.0218	0.00433	± 0.00023	0.00011876	± 0.0000452	12.85166	± 0.05114	99.72	232.36 ± 0.87	99.2	5.15	
MAA3389	7.8382	± 0.0169	0.00209	± 0.00039	0.00026206	± 0.0000839	7.75960	± 0.06031	99.00	143.79 ± 1.07	205.3	1.58	
MAA3391	96.8326	± 0.2066	0.00253	± 0.00037	0.00000256	± 0.0000861	96.83169	± 0.41643	100.00	1286.84 ± 3.97	170.0	22.08	
MAA3392	65.9480	± 0.1289	0.00147	± 0.00037	0.00038218	± 0.0000925	65.83351	± 0.26317	99.83	964.13 ± 3.00	292.7	13.97	
MAA3394	2.6494	± 0.0060	0.00895	± 0.00043	0.00011514	± 0.0000675	2.61519	± 0.04200	98.71	49.73 ± 0.79	48.1	0.67	
MAA3395	3.2970	± 0.0080	0.00306	± 0.00035	0.00011273	± 0.0000856	3.26309	± 0.05350	98.97	61.85 ± 1.00	140.6	0.64	
MAA3397	95.8149	± 0.1603	0.00331	± 0.00027	0.00051954	± 0.0000614	95.65970	± 0.32215	99.84	1275.62 ± 3.09	130.0	32.82	
MAA3398	76.9668	± 0.1872	0.00116	± 0.00044	0.00041005	± 0.0000947	76.84398	± 0.37803	99.84	1085.37 ± 4.03	371.0	14.21	
MAA3400	10.8729	± 0.0218	0.00294	± 0.00040	0.00034609	± 0.0000915	10.76926	± 0.06970	99.05	196.66 ± 1.21	146.0	2.19	
MAA3401	76.9950	± 0.1944	0.00411	± 0.00065	0.00051714	± 0.0001189	76.84060	± 0.39454	99.80	1085.34 ± 4.20	104.5	11.67	
MAA3403	94.1338	± 0.2122	0.00178	± 0.00040	0.00011695	± 0.0001005	94.09857	± 0.42848	99.96	1260.56 ± 4.15	241.1	18.60	
MAA3404	53.1049	± 0.0917	0.00055	± 0.00026	0.00014928	± 0.0000608	53.05983	± 0.18691	99.92	812.60 ± 2.31	787.3	14.65	
										No weighted mean age			

Laser - Single crystal fusion

Sample: BR-4 J-value: 0.0105290 ± 0.0000053 (2σ)

Material: sanidine and orthoclase

File	$^{40}Ar/^{39}Ar$	±1σ	$^{39}Ar/^{39}Ar$	±1σ	$^{36}Ar/^{39}Ar$	±1σ	$^{40}Ar^*/^{39}Ar_K$	± 2σ	% $^{40}Ar^*$	Age (Ma) ± 2σ (Ma)	K/Ca	$^{40}Ar^*$ (x e-15 mol)	Included in wtd. Mean
MAA3574	7.0535	± 0.0145	0.00687	± 0.00048	0.00002067	± 0.0000511	7.04732	± 0.04213	99.91	131.02 ± 0.76	62.6	1.60	
MAA3575	2.6218	± 0.0057	0.00771	± 0.00041	0.00003759	± 0.0000364	2.61069	± 0.02459	99.57	49.64 ± 0.46	55.8	0.85	x
MAA3577	2.6160	± 0.0066	0.00465	± 0.00040	0.00005689	± 0.0000409	2.59881	± 0.02775	99.34	49.41 ± 0.52	92.4	0.72	x
MAA3578	73.7417	± 0.1787	0.00135	± 0.00031	0.00015680	± 0.0000549	73.69450	± 0.35858	99.94	1051.30 ± 3.89	319.1	22.08	
MAA3580	2.6222	± 0.0062	0.00594	± 0.00043	0.00008493	± 0.0000434	2.59674	± 0.02864	99.03	49.38 ± 0.54	72.5	0.72	x
MAA3581	2.7331	± 0.0060	0.00529	± 0.00037	0.00010627	± 0.0000412	2.70123	± 0.02730	98.83	51.33 ± 0.51	81.3	0.81	
MAA3583	2.8732	± 0.0103	0.01801	± 0.00103	0.00002127	± 0.0000949	2.86781	± 0.06026	99.81	54.45 ± 1.13	23.9	0.34	
MAA3584	114.9851	± 0.2413	0.00155	± 0.00038	0.00005588	± 0.0000753	114.96812	± 0.48466	99.99	1451.98 ± 4.23	278.1	26.78	
MAA3586	12.2170	± 0.1135	0.00207	± 0.00348	0.00004602	± 0.0006271	12.20289	± 0.43781	99.88	221.26 ± 7.48	207.4	0.22	
MAA3587	63.6550	± 0.1724	0.00188	± 0.00038	0.00016469	± 0.0000772	63.60557	± 0.34769	99.92	938.40 ± 4.01	228.3	13.11	
MAA3589	2.6225	± 0.0075	0.00814	± 0.00066	0.00011397	± 0.0000637	2.58860	± 0.04082	98.71	49.22 ± 0.77	52.8	0.52	x
MAA3590	2.6022	± 0.0066	0.00575	± 0.00051	0.00000498	± 0.0000571	2.60061	± 0.03661	99.94	49.45 ± 0.69	74.8	0.57	x
MAA3592	107.6185	± 0.2201	0.00464	± 0.00049	0.00019573	± 0.0000694	107.56020	± 0.44187	99.95	1386.23 ± 3.99	92.6	25.07	
MAA3593	10.1839	± 0.0259	0.02358	± 0.00074	0.00020003	± 0.0000833	10.12572	± 0.07156	99.43	185.44 ± 1.25	18.2	1.50	
MAA3595	2.6110	± 0.0069	0.00673	± 0.00053	0.00007648	± 0.0000663	2.58819	± 0.04190	99.13	49.22 ± 0.79	63.9	0.51	x
MAA3596	2.6440	± 0.0096	0.01590	± 0.00090	0.00009529	± 0.0001194	2.61634	± 0.07382	98.95	49.74 ± 1.38	27.0	0.31	x
MAA3598	3.3061	± 0.0082	0.00203	± 0.00036	0.00009427	± 0.0000582	3.27759	± 0.03839	99.14	62.10 ± 0.72	211.7	0.74	
MAA3599	2.6033	± 0.0072	0.00697	± 0.00054	0.00000625	± 0.0000702	2.60149	± 0.04428	99.93	49.46 ± 0.83	61.7	0.47	x
MAA3601	2.6241	± 0.0060	0.01074	± 0.00075	0.00012665	± 0.0000775	2.58660	± 0.04781	98.57	49.19 ± 0.90	40.0	0.43	x
MAA3602	5.4820	± 0.0111	0.00535	± 0.00043	0.00015625	± 0.0000724	5.43526	± 0.04852	99.15	101.87 ± 0.88	80.4	1.27	
									Weighted mean age (9 of 20):		49.43 ± 0.23	MSWD:	0.24

Laser - Single crystal fusion

Sample: BR-3 J-value: 0.0105290 ± 0.0000053 (2σ)

Material: sanidine and orthoclase

File	$^{40}Ar/^{39}Ar$	±1σ	$^{39}Ar/^{39}Ar$	±1σ	$^{36}Ar/^{39}Ar$	±1σ	$^{40}Ar^*/^{39}Ar_K$	± 2σ	% $^{40}Ar^*$	Age (Ma)	± 2σ (Ma)	K/Ca	$^{40}Ar^*$ (x e-15 mol)	Included in wtd. Mean
MAA3574	2.6089	± 0.0073	0.00948	± 0.00218	0.00022367	± 0.0001312	2.54233	± 0.07965	97.45	48.35	± 1.50	45.4	0.51	x
MAA3575	2.9980	± 0.0110	0.01699	± 0.00355	0.00117247	± 0.0002412	2.64882	± 0.14543	88.35	50.35	± 2.73	25.3	0.34	x
MAA3577	2.6037	± 0.0070	0.00905	± 0.00172	0.00003287	± 0.0000981	2.59411	± 0.06022	99.63	49.33	± 1.13	47.5	0.62	x
MAA3578	2.6106	± 0.0067	0.01507	± 0.00211	0.00008860	± 0.0001061	2.58485	± 0.06474	99.01	49.15	± 1.21	28.5	0.64	x
MAA3580	11.4710	± 0.0609	0.00080	± 0.00816	0.00035433	± 0.0004892	11.36474	± 0.31612	99.07	206.89	± 5.44	537.2	0.56	
MAA3581	2.7052	± 0.0102	0.01298	± 0.00407	0.00042143	± 0.0002427	2.57995	± 0.14627	95.37	49.06	± 2.74	33.1	0.27	x
MAA3583	2.6669	± 0.0068	0.00588	± 0.00290	0.00021886	± 0.0001275	2.60153	± 0.07729	97.55	49.47	± 1.45	73.2	0.51	x
MAA3584	3.3980	± 0.0088	0.00873	± 0.00269	0.00261367	± 0.0001540	2.61786	± 0.09310	77.04	49.77	± 1.75	49.2	0.60	x
MAA3586	2.7783	± 0.0106	0.00708	± 0.00430	0.00061945	± 0.0002534	2.59344	± 0.15265	93.34	49.31	± 2.86	60.7	0.27	x
MAA3587	2.6099	± 0.0087	0.00396	± 0.00320	0.00008205	± 0.0001509	2.58520	± 0.09177	99.05	49.16	± 1.72	108.7	0.42	x
MAA3589	2.5925	± 0.0073	0.01577	± 0.00182	0.00001378	± 0.0001246	2.58914	± 0.07578	99.87	49.23	± 1.42	27.3	0.54	x
MAA3590	2.5917	± 0.0057	0.00720	± 0.00152	0.00012454	± 0.0000775	2.55461	± 0.04766	98.57	48.59	± 0.89	59.7	0.74	x
MAA3592	2.5950	± 0.0062	0.00808	± 0.00215	0.00005383	± 0.0001098	2.57903	± 0.06668	99.38	49.04	± 1.25	53.2	0.57	x
MAA3593	2.6100	± 0.0077	0.02444	± 0.00325	0.00036977	± 0.0001546	2.50106	± 0.09352	95.82	47.58	± 1.76	17.6	0.42	x
MAA3595	2.7683	± 0.0086	0.00737	± 0.00239	0.00029210	± 0.0001461	2.68119	± 0.08885	96.85	50.96	± 1.67	58.3	0.46	x
MAA3596	5.4524	± 0.0170	0.01104	± 0.00329	0.00040208	± 0.0001903	5.33274	± 0.11840	97.80	100.00	± 2.16	38.9	0.69	
MAA3598	2.6552	± 0.0082	0.01101	± 0.00362	0.00065428	± 0.0002237	2.46019	± 0.13448	92.66	46.81	± 2.53	39.1	0.30	x
MAA3599	2.6177	± 0.0060	0.00750	± 0.00147	0.00036452	± 0.0001001	2.50893	± 0.06088	95.85	47.73	± 1.14	57.4	0.65	x
MAA3601	2.6065	± 0.0054	0.00331	± 0.00132	0.00004975	± 0.0000677	2.59141	± 0.04185	99.42	49.28	± 0.79	130.0	1.01	x
MAA3602	2.6033	± 0.0072	0.00621	± 0.00256	0.00009375	± 0.0001556	2.57531	± 0.09402	98.92	48.97	± 1.76	69.3	0.44	x
									Weighted mean age (18 of 20):	48.98	± 0.38	MSWD:	1.20	

Values have been corrected for instrument background, source mass bias, detector efficiency, and decay of ^{37}Ar and ^{39}Ar

All dates in this table are relative to 28.201 Ma for the Fish Canyon sanidine standard

Atmospheric argon ratios			
$^{40}Ar/^{36}Ar$	298.56	± 0.31	Lee et al. (2006)
$^{38}Ar/^{36}Ar$	0.1885	± 0.0003	Lee et al. (2006)

Interfering isotope production ratios		
$(^{40}Ar/^{39}Ar)_K$	$(5.4 \pm 1.4) \times 10^{-4}$	Jicha & Brown (2014)
$(^{38}Ar/^{39}Ar)_K$	$(1.210 + 0.002) \times 10^{-2}$	Jicha & Brown (2014)
$(^{39}Ar/^{37}Ar)_{Ca}$	$(6.95 \pm 0.09) \times 10^{-4}$	Renne et al. (2013)
$(^{38}Ar/^{37}Ar)_{Ca}$	$(1.96 \pm 0.08) \times 10^{-5}$	Renne et al. (2013)
$(^{36}Ar/^{37}Ar)_{Ca}$	$(2.65 \pm 0.022) \times 10^{-4}$	Renne et al. (2013)

Decay constants		
l_{40Ar}	$(0.580 \pm 0.014) \times 10^{-10}$ a^{-1}	Min et al. (2000)
l_{β^-}	$(4.884 \pm 0.099) \times 10^{-10}$ a^{-1}	Min et al. (2000)
^{39}Ar	$(2.58 \pm 0.03) \times 10^{-3}$ a^{-1}	
^{37}Ar	$(8.23 \pm 0.042) \times 10^{-4}$ h^{-1}	
^{36}Cl	$(2.303 \pm 0.046) \times 10^{-6}$ a^{-1}	

Supplemental Figures:

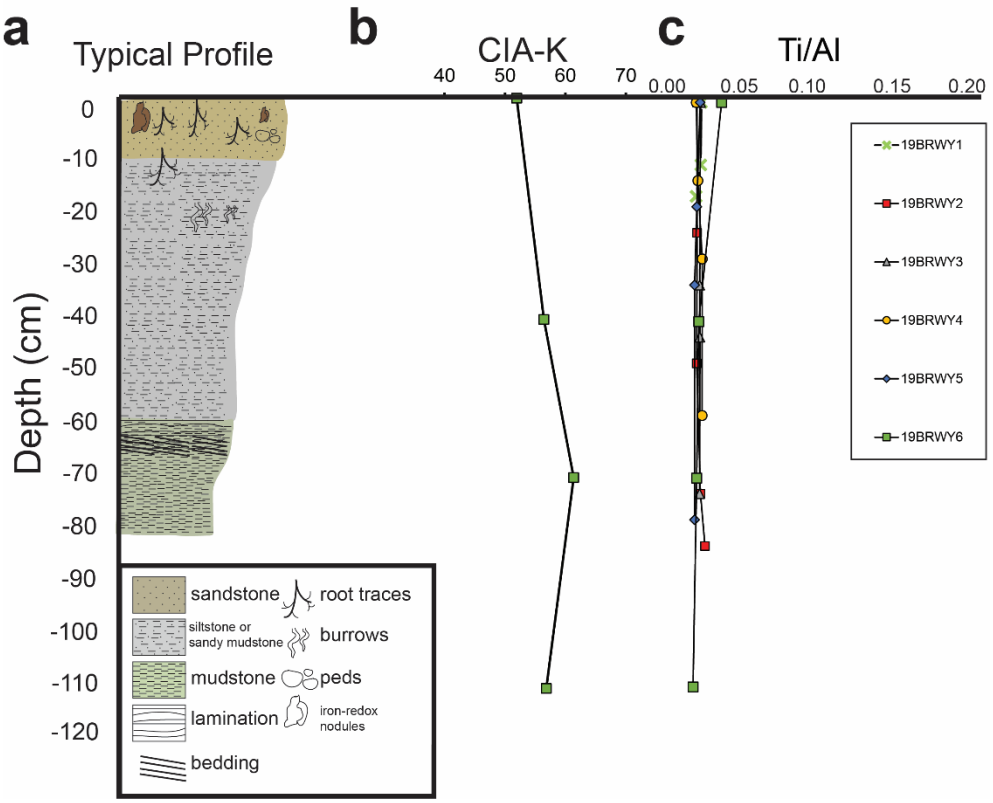

Figure S1 Paleosol features and elements. (a) Average paleosol profile at Blue Rim escarpment based on common horizon depths and features, (b) typical CIA-K over profile, (b) Ti/Al ratio (molar) for all paleosol profiles.

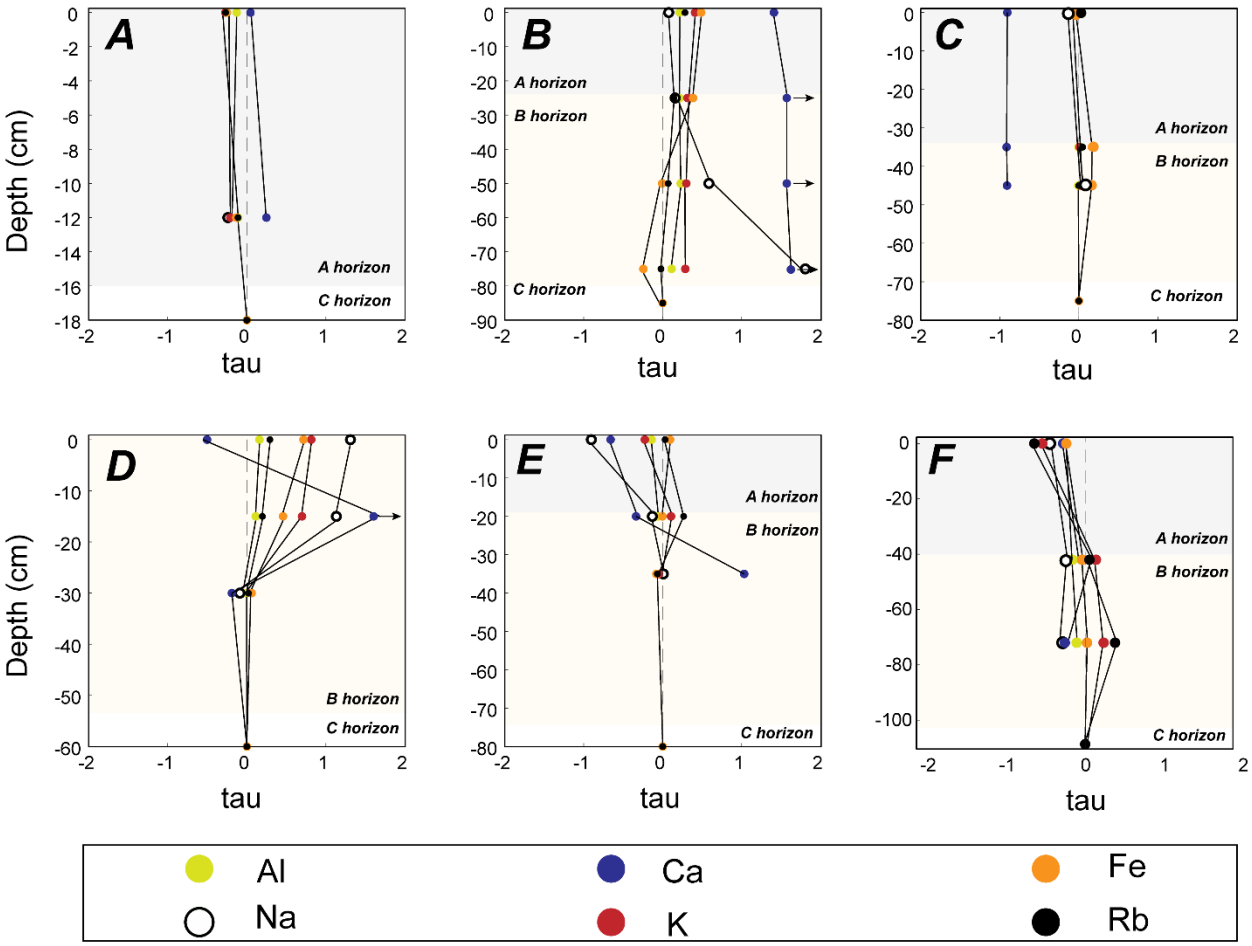

Figure S2 Up profile changes in tau (mobile element transport, see equations 2 and 3, per Chadwick et al. 1990) for Paleosols #1 (A) through #6 (F).

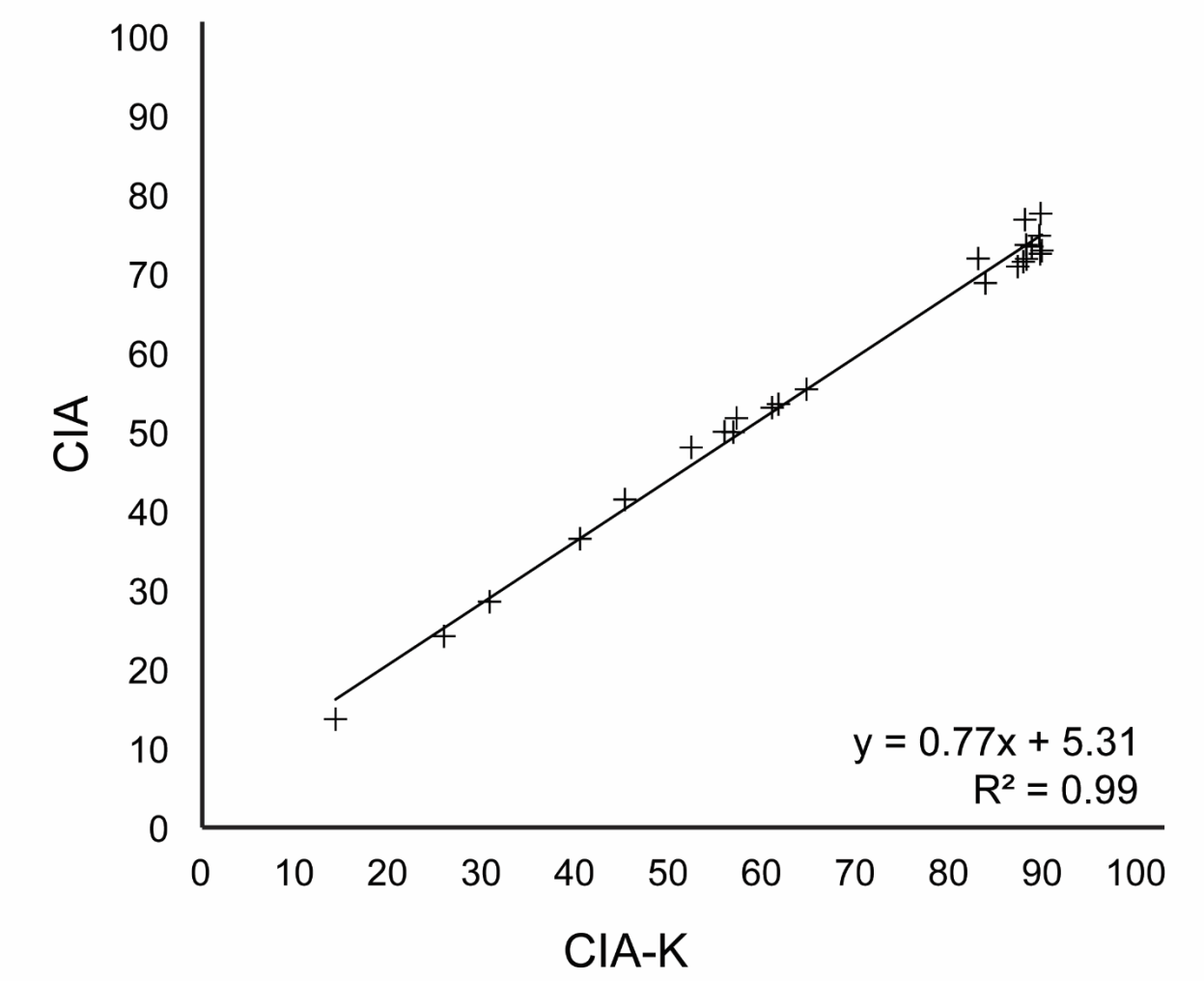

Figure S3 Relationship between CIA-K and CIA for all paleosol bulk geochemistry data, measured by ALS Laboratories in Vancouver, British Columbia, Canada.

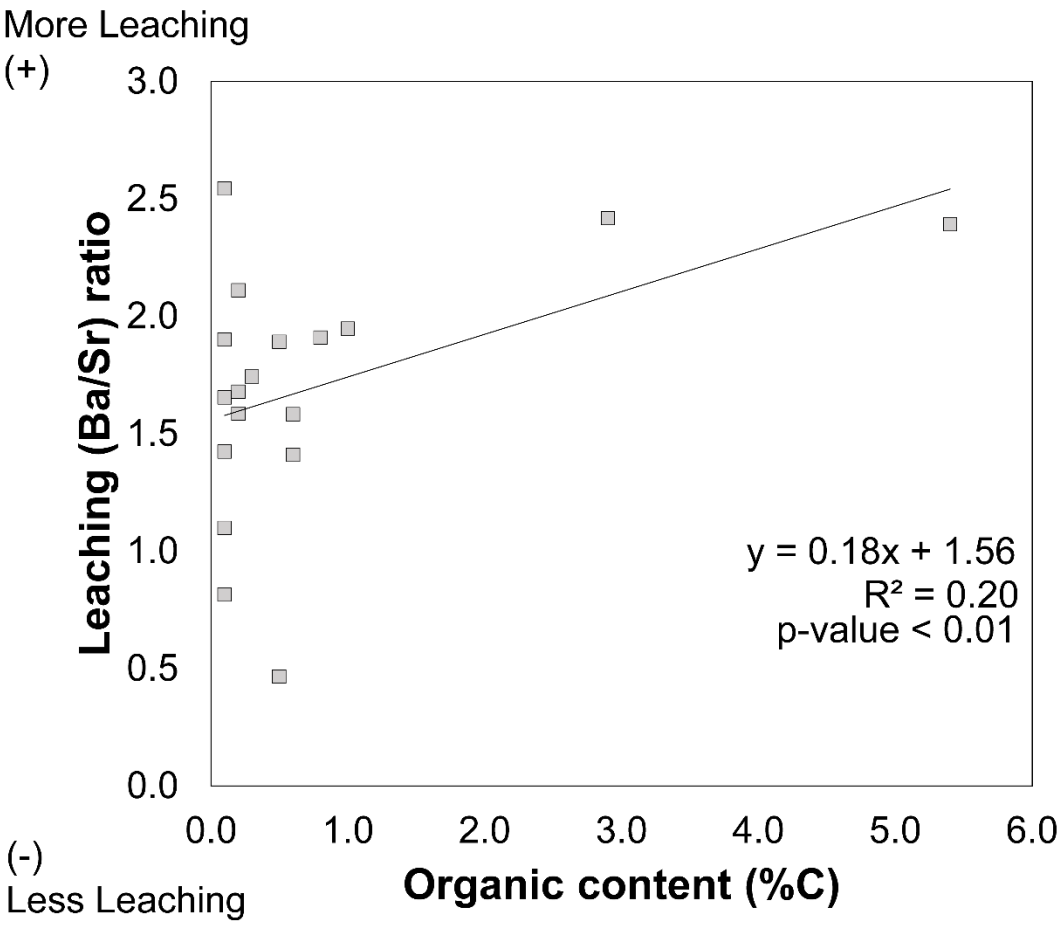

Figure S4 Comparison between organic content in stratigraphic units (%C) and leaching (Ba/Sr ratio).

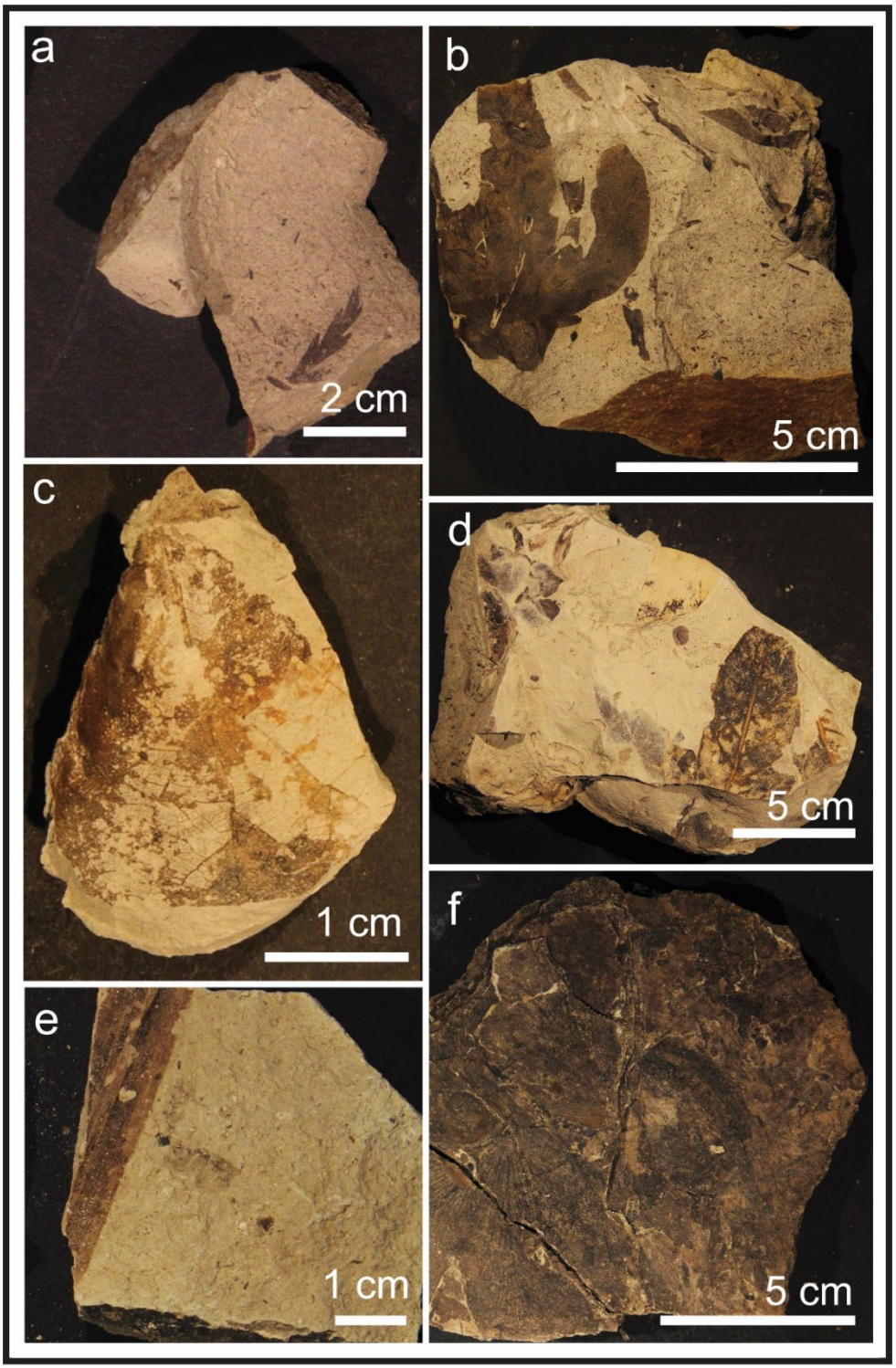

Figure S5 Common plant fossils and preservation types found at the Blue Rim Escarpment (2019): (a) *Lygodium kaulfussi,* (b) *Asplenium* sp. (c) *Populus cinnamomoides,* (d) cf. *Cedrela* sp. (e) unidentified monocot, (f) unidentified organ carbon-rich leaf mat, all sampled at 26 m in the section (see Figs. 3-5).

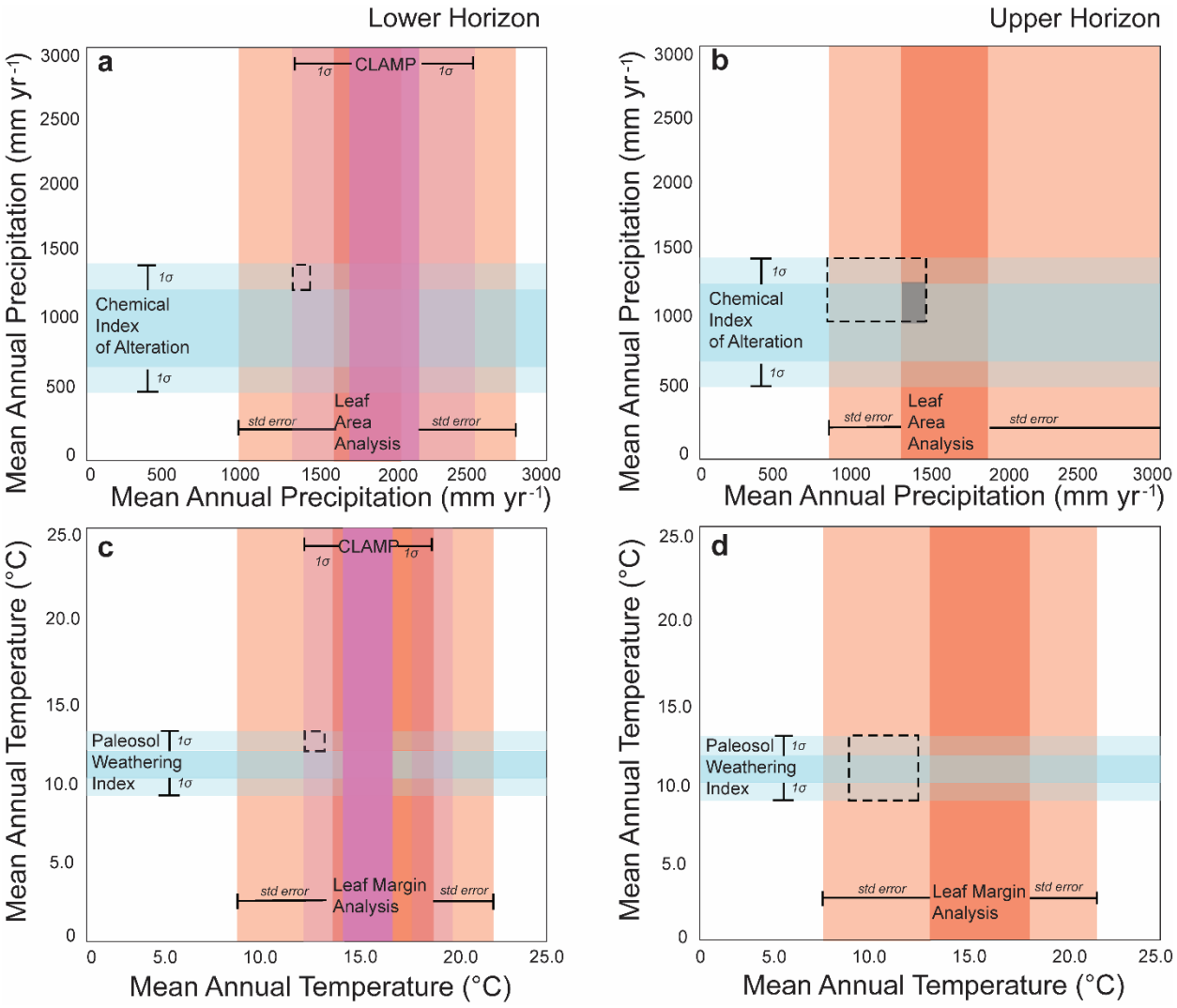

Figure S6 Comparisons of paleoclimate reconstructions using multiple proxies at Blue Rim, southwestern Wyoming. Paleosol-based proxies are shown in blue (y-axis), with opaque blue representing the range of reconstructed precipitation (a-b) and temperature (c-d) and transparent blue shows error for each proxy (1σ for Chemical Index of Alteration and Paleosol Weathering Index). Two plant-based proxies are shown in red (x-axis), with opaque red representing the range of reconstructed precipitation using leaf margin analysis and leaf area analysis based off multiple regional and global equations (e.g., Wolfe 1979; Wing & Greenwood 1993; Wilf 1997; Wilf et al., 1998; Gregory-Wodzicki 2000; Jacobs 2004; Kowalksi & Dilcher 2003; Miller et al., 2006; Peppe et al., 2011), and error (standard error) shown in opaque red. Climate Leaf Analysis Multivariate Program (CLAMP, a & c; e.g., Spicer et al. 2009) is shown in purple, with opaque purple to show the range of reconstructed values based on regional meteorological stations and global reconstructions, and transparent purple showing standard deviation (1σ). CLAMP was not done on the upper horizon. The precipitations and temperatures for which both proxies overlap (within error) are outlined in a dashed box, and grey boxes show the precipitations and temperatures that overlap for reconstructed ranges (excluding error). The Lower (plant macrofossil) Horizon is shown in panels a and c, the Upper (plant macrofossil) Horizon is shown in panels b and d (Allen, 2017b).

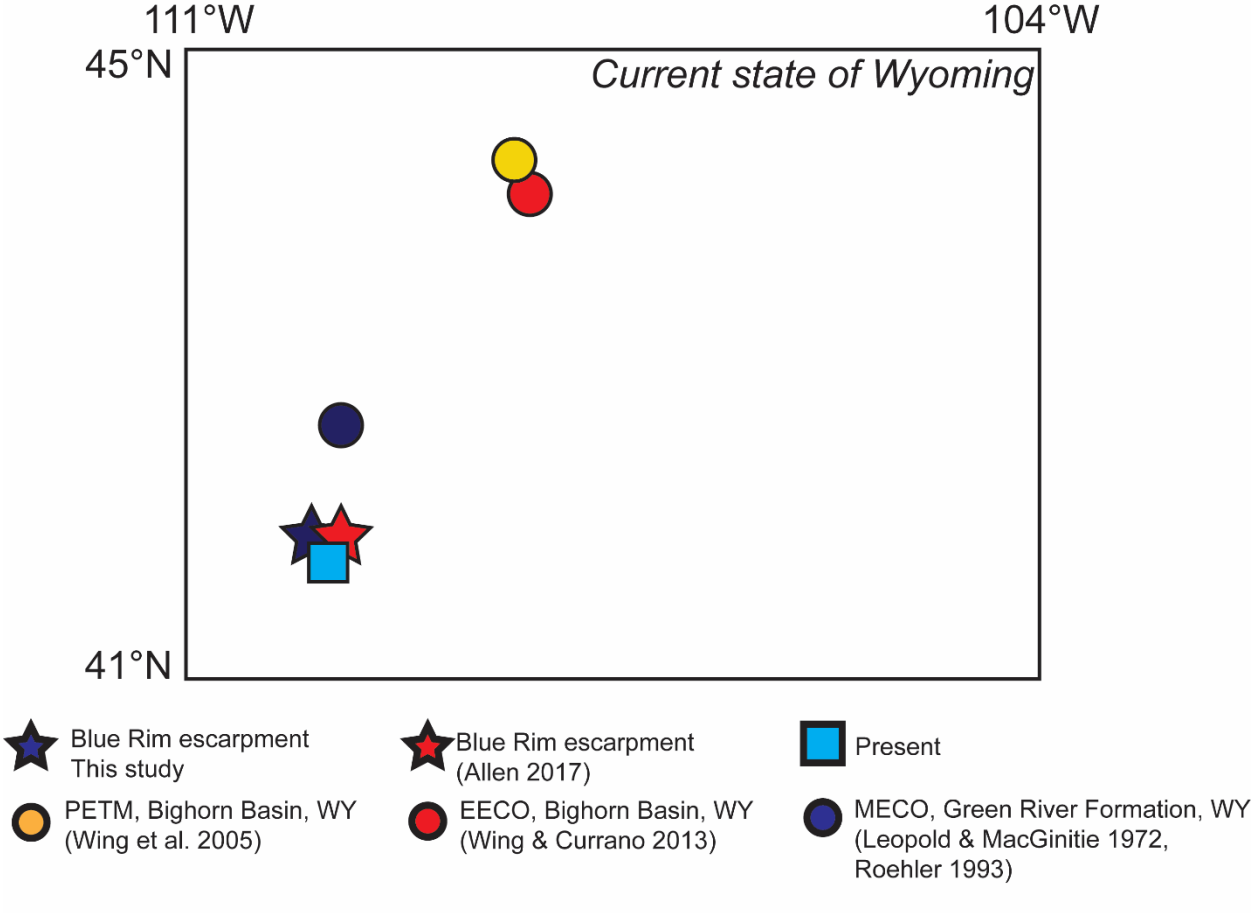

Figure S7 Current boundaries of Wyoming, USA with localities plotted with same symbols as seen in Figure 10. Blue Rim escarpment is plotted in stars (blue for this study, red for Allen 2017b). The Paleocene-Eocene Thermal Maximum record from Bighorn Basin is plotted in a yellow circle, while the EECO record from the Bighorn Basin is
plotted in a red circle. The middle Eocene climatic optimum (MECO) is plotted in a blue circle.

Supplemental Methods:

Floral humidity province

To contextualize climate variables (temperature, precipitation) to ecoregion and humidity, Gulbranson et al. (2011) developed a life-zone proxy based on Rasmussen et al. (2005) and Rasmussen and Tabor's (2007) pedogenic energy model. This energy quantifies energy influxes due to solar radiation (and subsequent net primary productivity: NPP) and precipitation. The total energy input into a soil (E_{in}) is related to energy supplied by NPP (E_{NPP}) and precipitation (E_{PPT}). E_{PPT} and E_{NPP} are calculated using weathering indices (CIA). E_{PPT} is plotted against evapotranspiration (ET) and divided into humidity zones using Eq. 9:

$$Equation\ (9) \quad ET = MAP - E_{PPT}\ [4.18(\Delta T)]^{-1}$$

Where ΔT is the temperature difference between 273.16 °K and mean annual temperature.

Mean annual precipitation calculated using the relationship between CIA-K and precipitation was used in this relationship (Eq. 5).

In modern environments, effective precipitation (Peff) is a linear function of MAP and ET (Eq. 10):

$$Equation\ (10) \qquad P_{eff} = MAP - ET$$

And Peff can be calculated using Eq. 11.

$$Equation\ (11) \qquad P_{eff} = 0.9075(MAP) - 21.403$$

Paleolatitude has been described as anywhere between 35 °N and 44 °N (Allen 2017b), which is necessary criteria for determining the best equation for E_{NPP} in Gulbranson et al.'s (2011) model, though temperature can be swapped out as the best fit criteria. Temperature has been described as 17-20 °C by prior studies for this region during this time (Allen 2017b), so we use Eq. 12 determined by ranges of MAT in Gulbranson et al. (2011).

$$Equation\ (12) \qquad E_{NPP} = -1.943(CIA)^2 + 352.41(CIA) + 28197$$

For reconstructed MAT and MAP values from alternate proxy data (non-paleosol estimates), CIA was back calculated estimating CIA-K using given precipitation values and Eq. 5, then translated into CIA values using Eq. 13.

This relationship was calculated using the relationship between CIA and CIA-K for all paleosol bulk geochemistry measurements at this site (Supplemental Fig. S1; $R^2 = 0.99$)

$$Equation\ (13) \quad CIA = 0.78(CIA - K) + 5.23$$

Holdridge Life Zones

The Holdridge Life Zone classification system (Holdridge 1947) matches climate with vegetation. Higher precipitation adds energy to a soil system, which mobilizes elements and weathers the soil. Evapotranspiration, represented on the other axis of the Holdridge biome diagram (Fig. 7b) represents energy loss from the soil profile. These two plotted together can then be divided into biome space, allowing for estimation of climate and vegetation through the same diagram. Using the ratio of evapotranspiration (calculated by Equation 10) to mean annual

precipitation, which represents potential evapotranspiration ratio, as compared to precipitation, we plotted each paleosol in life zones.

Global context of climate

Chronologically, the region of interest (specifically, the Rocky Mountain Wyoming region) went from wettest during the PETM in the proximal Bighorn Basin (rain forest; reconstructed using LMA and LAA; Wing et al. 2005) to drier and cooler (characterized as a wet forest), resulting in less evapotranspiration and less precipitation as time progressed. Blue Rim-era floral humidity provinces are all estimated to also be wet forests, which is further contextualized by fossil evidence as presented in the taxonomy and floral humidity provinces of our fossils and Allen's (2017) characterization of the escarpment. Other comparably aged Eocene climate reconstructions based on palynological data from the Laney Member of the Green River Formation (~48.5 Ma; Smith et al., 2008), located in the same basin as the Blue Rim escarpment, appear to be closer to rainforest floral humidity provinces (Leopold & MacGinitie 1972; Roehler 1993; Smith et al., 2008; Fig. 8). That being said, megaflora from the Green River Formation has been described as ranging from littoral to floodplain vegetation along the lakes edges, plants adapted to subhumid conditions slightly higher, broad-leaf deciduous trees in cooler and mesic situations, and conifer-hardwood and montane zones from high altitude regions (MacGinitie 1969). Over the late Paleogene into Neogene and more recently, the region has continued drying and is now high desert/dry scrub, with minimal precipitation (195 mm yr^{-1} in 2019, the year sampled; PRISM Climate Group 2004), cold winters (<0 °C from November to March; PRISM Climate Group 2004), and hot, dry summers (Fig. 8). The locations of each of these sites is plotted on Figure S7, to demonstrate their proximity.

The Parachute Creek, Laney, and Fossil Butte Members of the Green River Formation, all slightly older than the Blue Rim escarpment and deposited during the EECO, have also been interpreted as semi-deciduous with seasonally dry subtropical taxa (Wing 1987; Allen 2015). Further away in the Okanagan Highlands of the North American Pacific Northwest, climate reconstructions yield temperature ranges of 10–13.5 °C (Wolfe et al. 1994; Wolfe et al. 1998; Greenwood et al. 2005), similar to those values reconstructed at Blue Rim, demonstrating the equability of North America during the early Eocene.

Blue Rim climate based on floral vs paleosol reconstructions

Mean annual precipitation (MAP) reconstructions from this study based on inorganic proxies in paleosols ranged from 608–1167 mm yr^{-1} (average: 845 mm yr^{-1} ± 255 mm yr^{-1}, standard deviation). A high influence of carbonate in the parent material resulted in a lower CIA-K, and thus lower rainfall estimates (Sheldon et al. 2002). Error on CIA-K proxies is ± 181 mm yr^{-1} (Sheldon et al. 2002; Passchier et al. 2013), such that estimates from organic, physiognomic, and inorganic geochemical proxies are within error of one another. However, overall, these inorganic-based reconstructions are slightly lower than those estimated using Climate Leaf Analysis Multivariate Program (only in the lower horizon, CLAMP, 1653 ± 317 to 2070 ± 483 mm yr^{-1}; Allen 2017b) and leaf area analysis, which was estimated using four different regression equations based on different regions of today's world (LAA; ranging from 1299.4 + 563, -393 to 1539.8 + 1294, -703 depending on the regression used in the upper horizon: and 1454.8 + 358, -287 to 1711.0 + 1438, -781 depending on the regression used in UF-19404, isolated channel fill and oldest stratigraphically; Wilf et al. 1998; Gregory-Wodzicki 2000; Jacobs 2004; Peppe et al., 2011; Allen 2017b). This could be due to the location in the section

(stratigraphically older, see Figure 5) of the studied paleosols. Temperature results based off inorganic geochemistry in paleosols in this study were slightly lower than those reconstructed using leaf physiognomy (CLAMP: 14 to 15 °C, LMA: 14 to 20 °C; Fig. 7; Allen 2017b, originally calculated using Wolfe 1979; Wing and Greenwood 1993; Wilf 1997; Kowalski & Dilcher 2003; Miller et al., 2006; Spicer et al., 2009; and Peppe et al., 2011), with PWI-based temperatures ranging from 10 to 12 °C (average 11.0 °C ± 0.7 °C standard deviation; Fig. 7).